Tennessee Valley Authority, Post Office Box 2000, Decatur, Alabama 35609-2000

TVA-BFN-418

May 11, 2006

10 CFR 50.90

U.S. Nuclear Regulatory Commission
ATTN: Document Control Desk
Mail Stop: OWFN P1-35
Washington, D.C. 20555-0001

Gentlemen:

In the Matter of	)	Docket Nos. 50-260
Tennessee Valley Authority	)	50-296

BROWNS FERRY NUCLEAR PLANT (BFN) - UNITS 2 AND 3 - SUPPLEMENTAL RESPONSE TO NRC ROUND 3 REQUEST FOR ADDITIONAL INFORMATION (RAI) RELATED TO TECHNICAL SPECIFICATIONS (TS) CHANGE NO. TS-418 - EXTENDED POWER UPRATE OPERATION (EPU) (TAC NOS. MC3743 AND MC3744)

This letter provides a supplemental response to the Staff's December 22, 2005, Round 3 RAI (ADAMS Accession No. ML053560177) regarding the BFN Units 2 and 3 EPU license amendment applications, which were submitted on June 25, 2004 (ML041840301). TVA's response to the Round 3 RAI was submitted on March 7, 2006 (ML060680583).

NRC, TVA, and Areva subsequently met on April 26 and 27, 2006, at the Areva offices in Richland, Washington, and discussed several of the individual March 7, 2006, RAI responses. In that meeting, TVA agreed to clarify four of the SRXB RAI responses to support NRC's review of the Units 2 and 3 EPU license amendment applications. Enclosure 1 provides revised responses to four SRXB RAIs and also lists the six RAI responses that NRC indicated were satisfactory.

D030

To facilitate NRC review for the four revised responses, the entire original (March 7, 2006) RAI response, which includes the agreed to revisions, is provided in the enclosures.

Some of the information in Enclosure 1 is proprietary to Framatome (now known as Areva) and Areva requests that the proprietary information in this enclosure be withheld from public disclosure. An affidavit supporting this request is included in Enclosure 1. A non-proprietary version of this supplemental response is contained in Enclosure 2.

There are no new regulatory commitments associated with this submittal. If you have any questions concerning this letter, please contact me at (256) 729-2636.

I declare under penalty of perjury that the foregoing is true and correct. Executed on this 11th day of May, 2006.

Sincerely,

William D. Crouch
Manager of Licensing
and Industry Affairs

Enclosures:

1. Supplemental Response To NRC Round 3 Request For Additional Information (RAI) Related To Technical Specifications (TS) Change No. TS-418 - Request For Extended Power Uprate (EPU) Operation (Proprietary Version)

2. Supplemental Response To NRC Round 3 Request For Additional Information (RAI) Related To Technical Specifications (TS) Change No. TS-418 - Request For Extended Power Uprate (EPU) Operation (Non-Proprietary Version)

cc: See page 3

cc (Enclosures):

State Health Officer
Alabama Department of Public Health
RSA Tower - Administration
Suite 1552
P.O. Box 303017
Montgomery, Alabama 36130-3017

U.S. Nuclear Regulatory Commission
Region II
Sam Nunn Atlanta Federal Center
61 Forsyth Street, SW, Suite 23T85
Atlanta, Georgia 30303-8931

NRC Senior Resident Inspector
Browns Ferry Nuclear Plant
10833 Shaw Road
Athens, Alabama 35611-6970

Eva A. Brown, Project Manager
U.S. Nuclear Regulatory Commission
(MS 08G9)
One White Flint, North
11555 Rockville Pike
Rockville, Maryland 20852-2739

Margaret Chernoff, Project Manager
U.S. Nuclear Regulatory Commission
(MS 08G9)
One White Flint, North
11555 Rockville Pike
Rockville, Maryland 20852-2739

ENCLOSURE 2

TENNESSEE VALLEY AUTHORITY
BROWNS FERRY NUCLEAR PLANT (BFN)
UNITS 2 AND 3

SUPPLEMENTAL RESPONSE TO NRC ROUND 3 REQUEST FOR ADDITIONAL INFORMATION (RAI) RELATED TO TECHNICAL SPECIFICATIONS (TS) CHANGE NO. TS-418 - REQUEST FOR EXTENDED POWER UPRATE (EPU) OPERATION

(NON-PROPRIETARY VERSION)

ENCLOSURE 2

TENNESSEE VALLEY AUTHORITY
BROWNS FERRY NUCLEAR PLANT (BFN)
UNITS 2 AND 3

SUPPLEMENTAL RESPONSE TO NRC ROUND 3 REQUESTS FOR ADDITIONAL INFORMATION (RAI) RELATED TO TECHNICAL SPECIFICATIONS (TS) CHANGE NO. TS-418 - REQUEST FOR EXTENDED POWER UPRATE (EPU) OPERATION

(NON-PROPRIETARY VERSION)

This enclosure provides a supplemental response to the Staff's December 22, 2005, Round 3 RAI (ADAMS Accession No. ML053560177) regarding the BFN Units 2 and 3 EPU license amendment applications, which were submitted on June 25, 2004 (ML041840301). TVA's response to the RAI Round 3 was submitted on March 7, 2006 (ML060680583).

NRC, TVA, and Areva subsequently met on April 26 and 27, 2006, at the Areva offices in Richland, Washington, to discuss the March 7, 2006 RAI response (meeting notice ML061030509). In the meeting, the TVA responses to ten of the individual RAI responses (SRXB-A.26 through SRXB-A.35), which are associated with Areva analysis methodology, were discussed in detail. As a result, TVA agreed to clarify four of the subject SRXB RAI responses to better support NRC's review of the Units 2 and 3 EPU license amendment applications. This enclosure provides the revised responses to the four SRXB RAIs and also lists the remaining six RAI responses that NRC indicated were satisfactory. To facilitate NRC review, for the four revised responses, the entire original (March 7, 2006) RAI response including revisions is provided.

SBWB (SRXB-A)

SRXB-A.26 (Response Satisfactory)

NRC Request SRXB-A.27

Demonstrate quantitatively and qualitatively, that the current uncertainties and biases established in the benchmarkings and presented in Table 9.8 and 9.9 of EMF-2158(P)-A remain valid for the neutronic and thermal-hydraulic conditions predicted for the EPU operation. Specifically, demonstrate the uncertainties and biases used in your reactivity coefficients (e.g., void coefficient) are applicable or remain valid for the neutronic and thermal-hydraulic conditions expected for EPU operation.

TVA Reply to SRXB-A.27- Revised

FANP has reviewed the data presented in EMF-2158(P)(A) with regard to the maximum assembly power (Figure SRXB-A.27-1) and maximum exit void fraction (Figure SRXB-A.27-2) to determine the range of data previously benchmarked. This data can be compared to the equivalent data of the analysis performed for BFN operating under EPU and non-EPU conditions (Figures SRXB-A.27-3 and 27-4). It should be noted that the data provided includes actual operating data as well as projections for future operation. The case of BFN Unit 1 Cycle 9 is a hypothetical situation performed as a scoping study. Comparison of Figure 27-1 vs. Figure 27-3 and Figure 27-2 vs. Figure 27-4 shows that EPU operation in the standard power/flow map as well as MELLLA+ is within the range of the original methodology approval for assembly power and exit void fraction. From a neutronic perspective, moderator density (void fraction) and exposure cause the greatest variation in cross sections. The exposure range is defined in the mechanical evaluation model discussed in response SRXB-A.16 and is unchanged between non-EPU and EPU conditions. Variations in cross sections are the main source of uncertainties. Since the range of void fraction for EPU operation is the same as the range in the topical report, the power distribution uncertainties determined in the topical report EMF-2158(P)(A) are applicable.

Fuel loading patterns and operating control rod patterns are constrained by the MCPR limit, which consequently limits the assembly power and exit void fraction regardless of the core power level. The axial profile of the power and void fraction of the limiting assembly and core average values are presented in Figures SRXB-A.27-5 and 27-6 for the BFN Unit 3 Cycle 12 design and a hypothetical EPU cycle design. These profiles demonstrate that the core average void fraction increases with EPU, however, the maximum assembly power does not produce any larger void fractions.

Another measure of the thermal-hydraulic conditions is the population distribution of the void fractions. Figures SRXB-A.27-7 and 27-8 present histograms of the void fraction for non-EPU and EPU conditions. These histograms were taken at the point of maximum exit void fraction expected during the cycle. The distribution of voids is shifted toward the 70 to 80% void fraction levels. The population of nodes experiencing 85 to 90% voids is still small.

The EMF-2158(P)(A) data was also re-evaluated by looking at the deviations between measured and calculated Traversing Incore

Probe (TIP) response for each axial level. The standard deviation of these deviations at each axial plane are presented in Figure SRXB-A.27-9 and demonstrates that there is no significant trend versus axial position, which indicates no significant trend versus void fraction.

Pin-by-pin gamma scan data is used for verification of the local peaking factor uncertainty. Quad Cities 1 measurements presented in the topical report EMF-2158(P)(A) have been re-evaluated to determine any axial dependency. Figure SRXB-A.27-10 presents the raw data including measurement uncertainty and demonstrates that there is no axial dependency. The more recent gamma scans performed by KWU, presented in the topical report EMF-2158(P)(A) and re-arranged by axial level in Table SRXB-A.27-1, indicate no axial dependency. Full axial scans were performed on 16 fuel rods. Comparisons to calculated data show excellent agreement at all axial levels. The dip in power associated with spacers, observed in the measured data, is not modeled in MICROBURN-B2. There is no indication of reduced accuracy at the higher void fractions.

The FANP methodology [[
]] the reactivity coefficients that are used in the transient analysis. Conservatisms in the methodology are used to produce conservative results. Data presented in these referenced figures indicate that there are no significant differences between EPU and non-EPU conditions that have an impact on the reactivity coefficients.

Table SRXB-A.27-1: KWU-S Gamma Scan Benchmark Results from EMF-2158(P)(A)

[[

]]

Figure SRXB-A.27-1: Maximum Assembly Power in Topical Report EMF-2158(P)(A)

[[

]]

Figure SRXB-A.27-2: Maximum Exit Void Fraction in Topical Report EMF-2158(P)(A)

[[

]]

Figure SRXB-A.27-3: Maximum Assembly Power in Browns Ferry Design

[[

]]

Figure SRXB-A.27-4: Maximum Exit Void Fraction in Browns Ferry Design

[[

]]

Figure SRXB-A.27-5: Browns Ferry Non-EPU Design Axial Profile of Power and Void Fraction

[[

]]

Figure SRXB-A.27-6: Browns Ferry EPU Design Axial Profile of Power and Void Fraction

[[

]]

Figure SRXB-A.27-7: Browns Ferry (Non-EPU) Nodal Void Fraction Histogram

[[

]]

Figure SRXB-A.27-8: Browns Ferry EPU Nodal Void Fraction Histogram

[[

]]

Figure SRXB-A.27-9: EMF-2158(P)(A) TIP Statistics by Axial Level

[[

]]

Figure SRXB-A.27-10: Quad Cities Unit 1 Pin-by-Pin Gamma Scan Results

[[

]]

SRXB-A.28 (Response Satisfactory)

SRXB-A.29 (Response Satisfactory)

NRC Request SRXB-A.30

Demonstrate that the Framatome-ANP neutronic methodology prediction capability for current fuel designs operated under the current operating strategies and core conditions. Prediction comparison should be made to gamma scans and traversing incore probe (TIP) core follow data. This demonstration applies to any recent fuel, such as the ATRIUM-9 and ATRIUM-10, in particular for first cycle and second cycle fuel. (Refer to Framatome Handout for August 4, 2005, Meeting; ADAMS Accession No. ML052370230.)

TVA Reply to SRXB-A.30 - Revised

Actual operating data from several recent fuel cycle designs have been evaluated and compared to that in the topical report EMF-2158(P)(A). Maximum assembly powers and maximum void fractions similar to that presented in the response to SRXB-A.27 are presented in Figures SRXB-A.30-1 and 30-2.

In order to evaluate some of the details of the void distribution, a current design calculation was reviewed in more detail. Figures SRXB-A.30-3 and 30-4 present the following parameters at the point of the highest exit void fraction (at 9336 MWd/MTU cycle exposure) in cycle core design for a BWR-6 reactor with ATRIUM-10 fuel. These are representative figures for a high power density plant and do not correspond to the data from Figures SRXB-A.30-1 and 30-2.

- Core average void axial profile
- Axial void profile of the peak assembly
- Histogram of the nodal void fractions in core

Reactor conditions for BFN with power uprate are not significantly different from that of current experience. The range of void fractions in the topical report data exceeds that expected for the power uprate conditions. The distribution of voids is nearly the same as current experience.

Gamma scan comparisons for 9X9-1 and ATRIUM-10 fuel were presented in the topical report, EMF-2158(P)(A), in section 8.2.2. Figures 8.18 through 8.31 show very good comparisons between the calculated and measured relative Ba-140 density distributions for both radial and axial values.

Data presented in these figures and tables demonstrate that the FANP methodology is capable of accurately predicting reactor conditions for fuel designs operated under the current operating strategies and core conditions.

Figure SRXB-A.30-1: Maximum Assembly Power Observed from Recent Operating Experience

[[

]]

Figure SRXB-A.30-2: Void Fractions Observed from Recent Operating Experience

[[

]]

Figure SRXB-A.30-3: Axial Power and Void Profile Observed from Recent Design Experience

[[

]]

Figure SRXB-A.30-4: Nodal Void Fraction Histogram Observed from Recent Design Experience

[[

]]

SRXB-A.31 (Response Satisfactory)

SRXB-A.32 (Response Satisfactory)

SRXB-A.33 (Response Satisfactory)

NRC Request SRXB-A.34

Describe qualitatively the cross-section reconstruction process incorporated in CASMO-4 and MICROBURN-B2. The response should reflect the information provided in the slides (1-35) of the August 4 presentations, including high void fraction effects and accuracy. Provide flow chart(s), road map(s) and any other means to demonstrate the process, starting from the gathered raw void fraction data, how that data is used by CASMO-4 to generate the required cross-sections. In addition, briefly describe the development of the void fraction correlation and associated uncertainties.

TVA Reply to SRXB-A.34 - Revised

CASMO-4 performs a multi-group [[ ]] spectrum calculation using a detailed heterogeneous description of the fuel lattice components. Fuel rods, absorber rods, water rods/channels and structural components are modeled explicitly. The library has cross sections for [[ ]] materials including [[ ]] heavy metals. Depletion is performed with a predictor-corrector approach in each fuel or absorber rod. The two-dimensional transport solution is based upon the [[ ]]. The solution provides pin-by-pin power and exposure distributions, homogeneous multi-group (2) microscopic cross sections, as well as macroscopic cross sections. Discontinuity factors are determined from the solution. [[ ]] gamma transport calculation are performed. The code has the ability to perform [[ ]] calculations with different mesh spacings. Reflector calculations are easily performed.

MICROBURN-B2 performs microscopic fuel depletion on a nodal basis. The neutron diffusion equation is solved with a full two energy group method. Modern nodal method solution using discontinuity factors is used along with a [[ ]]. The flux discontinuity factors are [[ ]]. A multilevel iteration technique is employed for efficiency. MICROBURN-B2 treats a total of [[ ]] heavy metal nuclides to account for the primary reactivity components. Models for nodal [[ ]] are used to improve the accurate representation of the in-reactor configuration. Full three dimensional pin power

reconstruction method is utilized. TIP (neutron and gamma) and Local Power Range Monitor (LPRM) response models are included to compare calculated and measured instrument responses. Modern steady state thermal hydraulics models define the flow distribution among the assemblies. [[
]] based upon CASMO-4 calculations are used for the in-channel fluid conditions as well as in the bypass and water rod regions. Modules for the calculation of CPR, LHGR and MAPLHGR are implemented for direct comparisons to the operating limits.

MICROBURN-B2 determines the nodal macroscopic cross sections by summing the contribution of the various nuclides.

$$\Sigma_x(\rho,\Pi,E,R)=\sum_{i=1}^{I}N_i\sigma_x^i(\rho,\Pi,E,R)+\Delta\Sigma_x^b(\rho,\Pi,E,R)$$

where:

Σ_x = nodal macroscopic cross section

$\Delta\Sigma_x^b$ = background nodal macroscopic cross section $(D, \Sigma_f, \Sigma_a, \Sigma_r)$

N_i = nodal number density of nuclide "i"

σ_x^i = microscopic cross section of nuclide "i"

I = total number of explicitly modeled nuclides

ρ = nodal instantaneous coolant density

Π = nodal spectral history

E = nodal exposure

R = control fraction

Functional representation of σ_x^i and $\Delta\Sigma_x^b$ comes from 3 void depletion calculations with CASMO-4. Instantaneous branch calculations at alternate conditions of void and control state are also performed. The result is a multi-dimensional table of microscopic and macroscopic cross sections. Figures SRXB-A.34-1 and 34-2 illustrate this with the thermal and fast microscopic cross sections for U235.

At Beginning of Life (BOL) the relationship is fairly simple, the cross section is only a function of void fraction (water density) and the reason for the variation is the change in the spectrum due to the water density variations. At any exposure point, a quadratic fit of the three CASMO-4 data points is used to represent the continuous cross section over instantaneous variation of void or water density. This fit is shown in Figures SRXB-A.34-3 and 34-4.

Detailed CASMO-4 calculations confirm that a quadratic fit accurately represents the cross sections as shown in Figures SRXB-A.34-5, 34-6, and 34-7.

With depletion the isotopic changes cause other spectral changes. Cross sections change due to the spectrum changes. Cross sections also change due to self-shielding as the concentrations change. These are accounted for by the void (spectral) history and exposure parameters. Exposure variations utilize a piecewise linear interpolation over tabulated values at [[ ]] exposure points. The four dimensional representation can be reduced to three dimensions (see Figure SRXB-A.34-8) by looking at a single exposure.

[[ ]] interpolation is performed in each direction independently for the most accurate representation. Considering the case at 70 GWd/MTU with an instantaneous void fraction of 70% and a historical void fraction of 60% Figures SRXB-A.34-9 and 34-10 illustrate the interpolation process. The table values from the library at 0.0, 0.4, and 0.8 void fractions are used to generate 3 quadratic curves representing the behavior of the cross section as a function of the historical void fraction for each of the tabular instantaneous void fractions (0.0, 0.4, and 0.8).

The intersection of the [[ ]] lines with the historical void fraction of interest are then used to create another [[ ]] fit in order to obtain the resultant cross section as shown in Figure SRXB-A.34-10.

The results of this process for all isotopes and all cross sections in MICROBURN-B2 were compared for an independent CASMO-4 calculation with continuous operation at 40% void (40% void history) and branch calculations at 90% void for multiple exposures. The results show very good agreement for the whole exposure range as shown in Figures SRXB-A.34-11 and 34-12.

At the peak reactivity point multiple comparisons were made (Figure SRXB-A.34-13) to show the results for various instantaneous void fractions.

Use of higher void fractions in CASMO-4 (for example 0,45,90) introduces more error for intermediate void fractions. Figure SRXB-A.34-14 shows the difference between a [[ ]] and a 0,45,90 interpolation method. Considering the better accuracy of the [[ ]] methodology for the majority of assemblies (less than 85% void), the current methodology [[

]] is considered appropriate for current and EPU conditions. The errors observed in the figure demonstrate that the errors [[ ]] are not significantly different from those seen with interpolation. This indicates that the uncertainties in the power distribution determined in EMF-2158(P)(A) are expected to be valid with [[ ]].

Void fraction has been used for the previous illustrations; however, MICROBURN-B2 uses water density rather than void fraction in order to account for pressure changes as well as subcooled density changes. This transformation does not change the basic behavior as water density is proportional to void fraction. MICROBURN-B2 uses spectral history rather than void history in order to account for other spectral influences due to actual core conditions (fuel loading, control rod inventory, leakage, etc.) The doppler feedback due to the fuel temperature is modeled by accumulating the Doppler broadening of microscopic cross sections of each nuclide.

[[

]]

The partial derivatives are determined from branch calculations performed with CASMO-4 at various exposures and void fractions for each void history depletion. The tables of cross sections include data for [[ ]] states. The process is the same for [[ ]] states. Other important feedbacks to nodal cross sections are lattice [[ ]] and instantaneous [[ ]] between lattices of different [[ ]]. These feedbacks are modeled in detail.

The methods used in CASMO-4 are state of the art. The methods used in MICROBURN-B2 are state of the art. The methodology accurately models a wide range of thermal-hydraulic conditions including EPU and MELLLA+ conditions.

The development of the void fraction correlation and the associated uncertainties are described in the response to SRXB-A.35.

Figure SRXB-A.34-1: Microscopic Thermal Cross Section of U-235 from Base Depletion and Branches

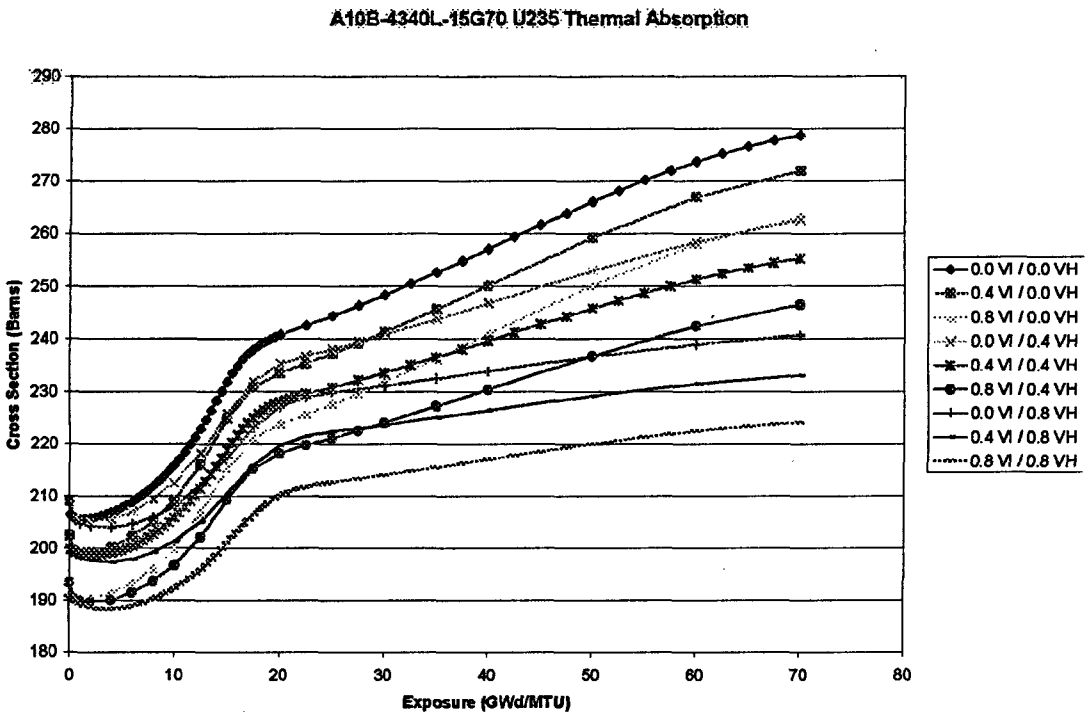

Figure SRXB-A.34-2: Microscopic Fast Cross Section of U-235 from Base Depletion and Branches

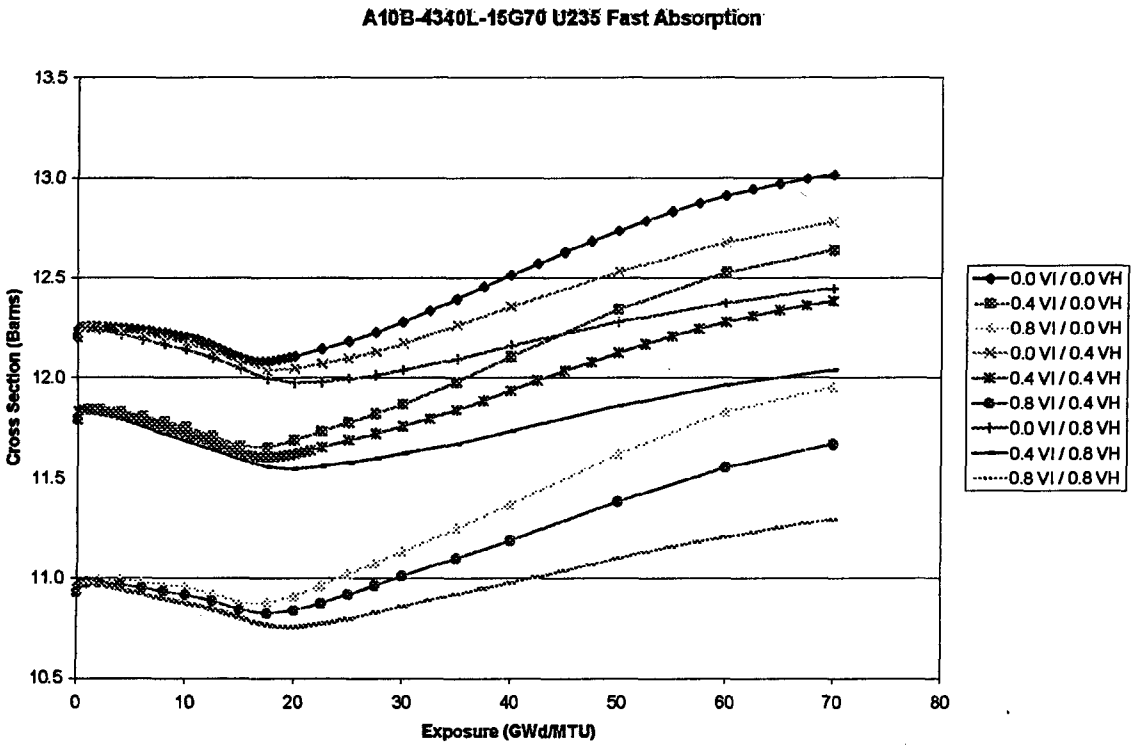

Figure SRXB-A.34-3: Microscopic Thermal Cross Section of U-235 at Beginning of Life

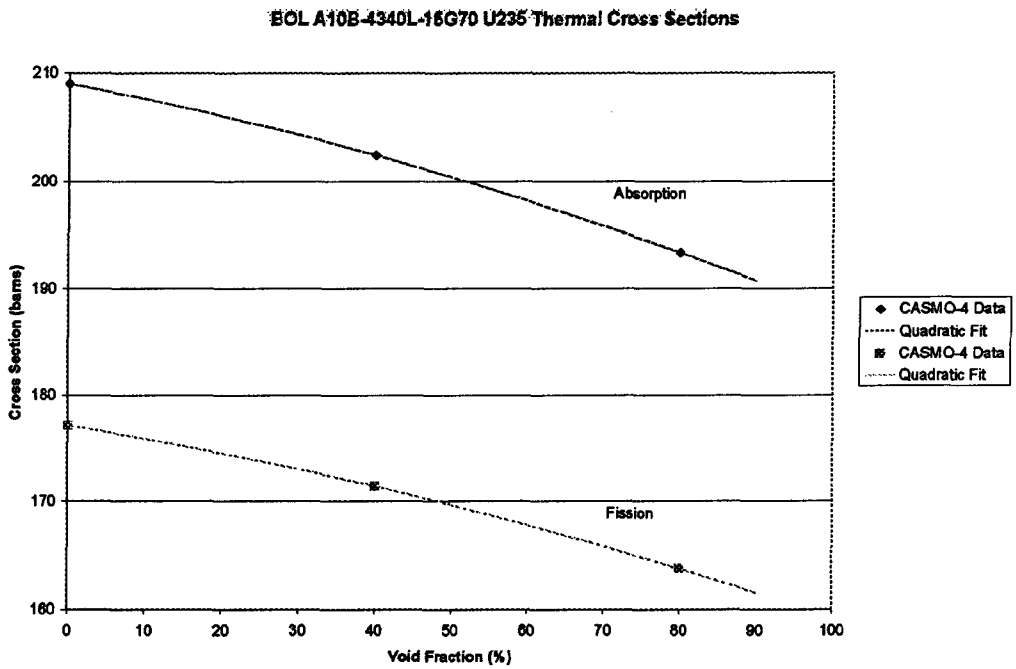

Figure SRXB-A.34-4: Microscopic Fast Cross Section of U-235 at Beginning of Life

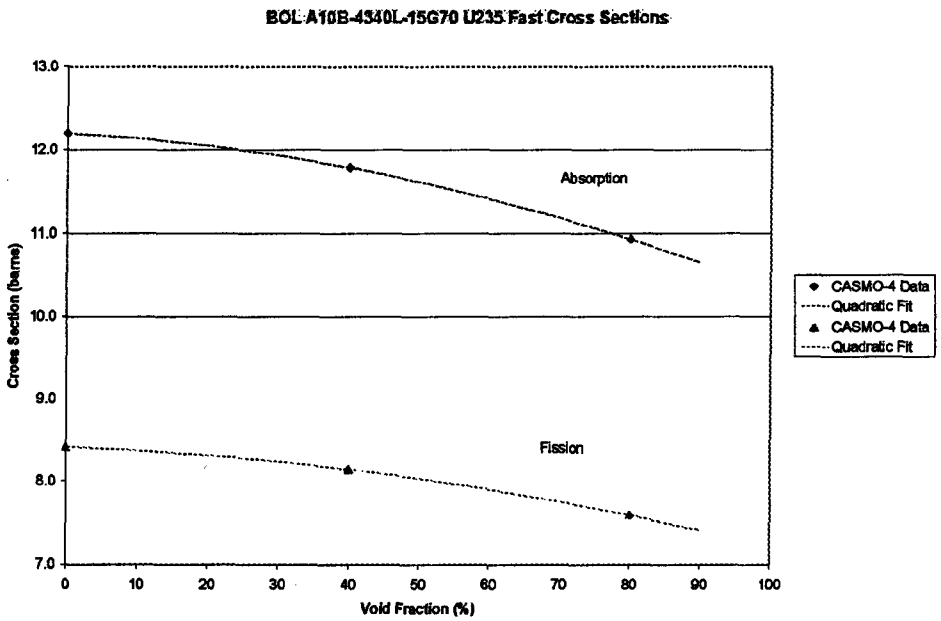

Figure SRXB-A.34-5: Microscopic Thermal Cross Section of U-235 Comparison of Quadratic Fit with Explicit Calculations at Various Void Fractions

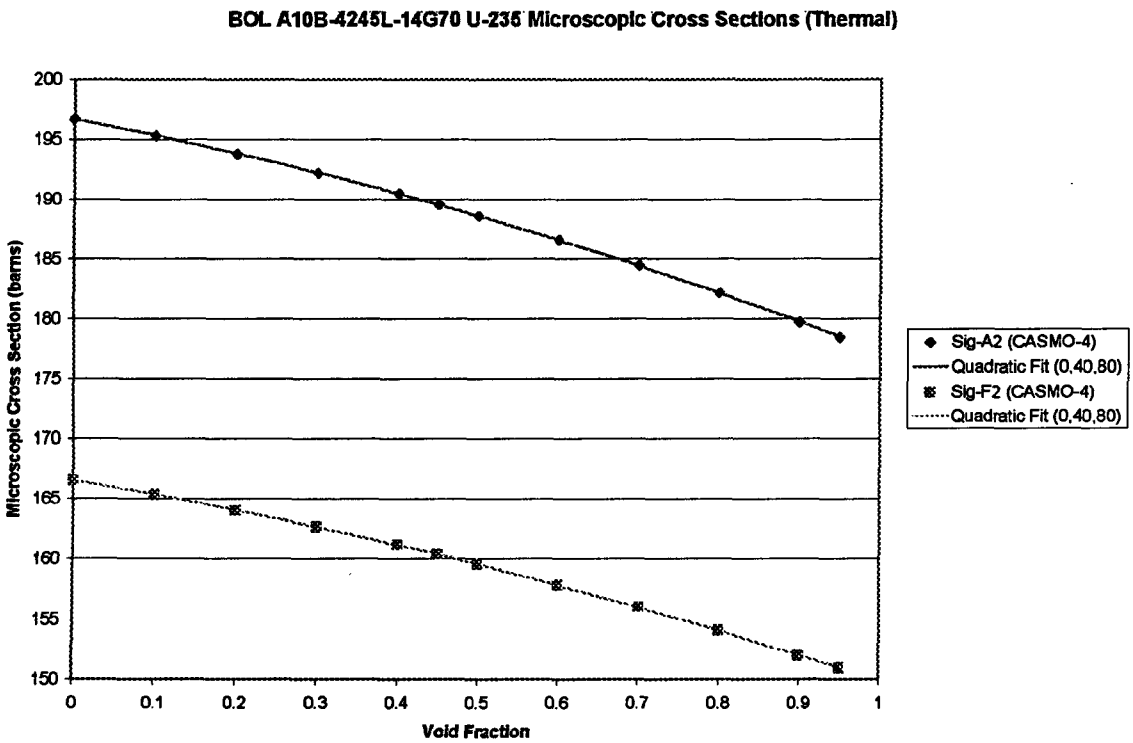

Figure SRXB-A.34-6: Microscopic Fast Cross Section of U-235 Comparison of Quadratic Fit with Explicit Calculations at Various Void Fractions

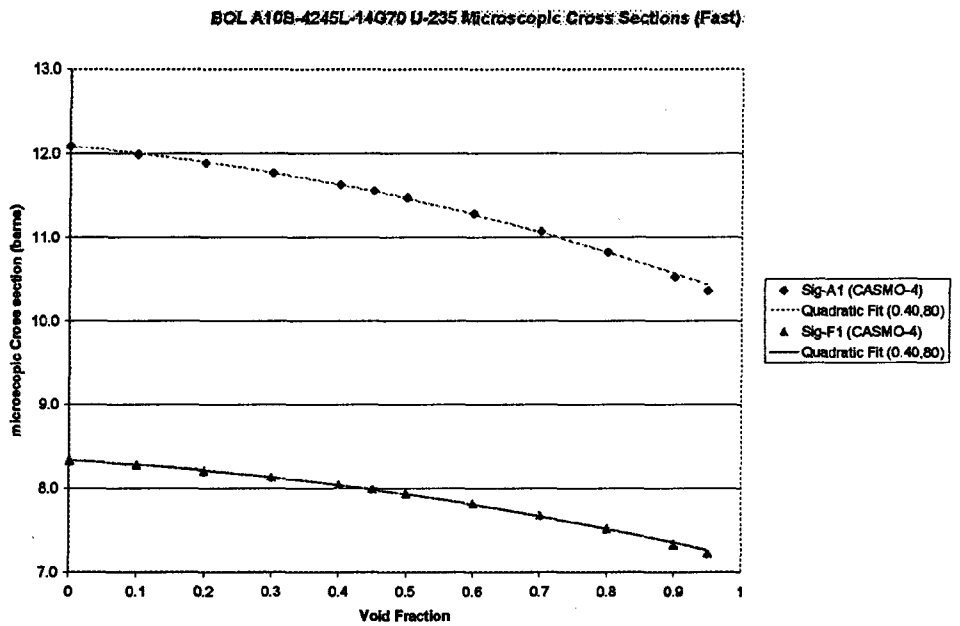

Figure SRXB-A.34-7: Macroscopic Diffusion Coefficient (Fast and Thermal) Comparison of Quadratic Fit with Explicit Calculations at Various Void Fractions

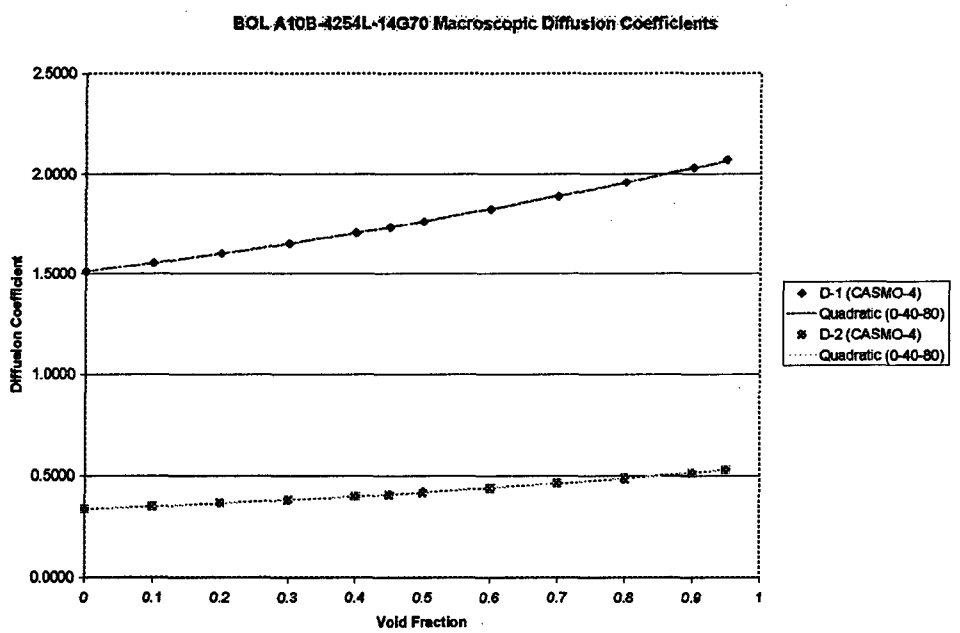

Figure SRXB-A.34-8: Microscopic Thermal Cross Section of U-235 at 70 GWd/MTU

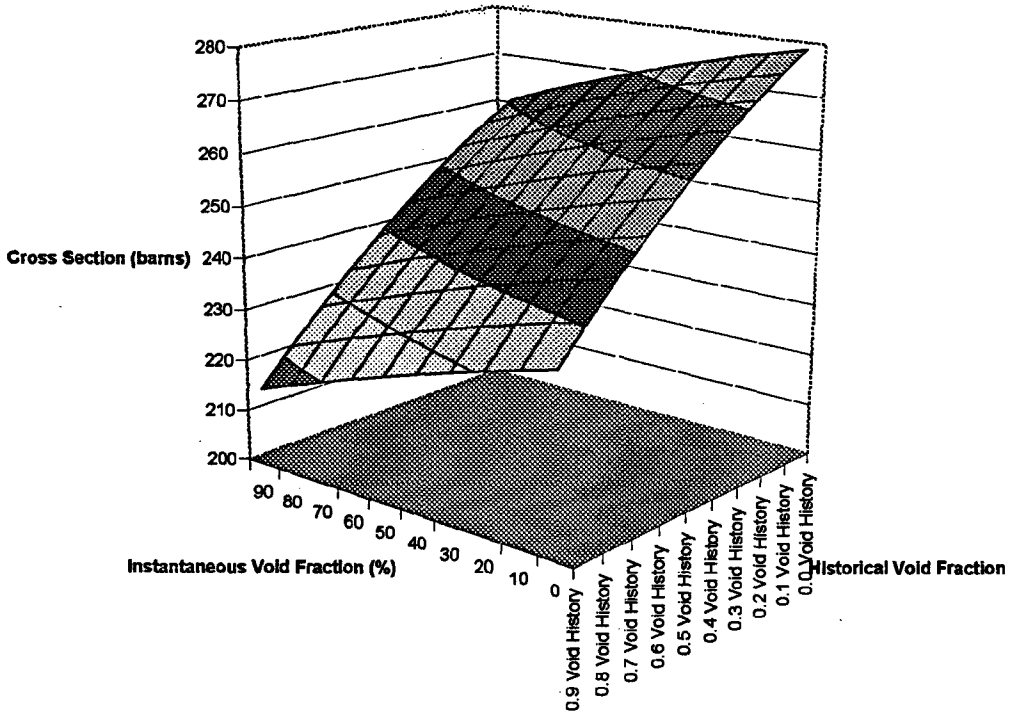

Figure SRXB-A.34-9: Quadratic Interpolation Illustration of Microscopic Thermal Cross Section of U-235

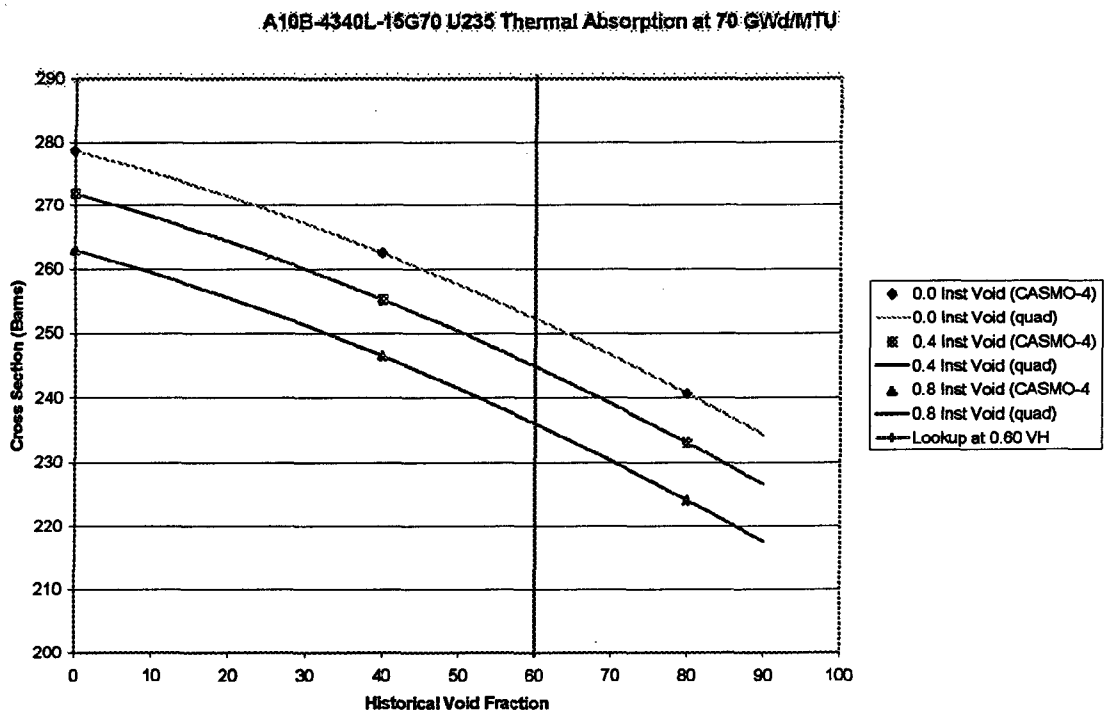

Figure SRXB-A.34-10: Illustration of Final Quadratic Interpolation for Microscopic Thermal Cross Section of U-235

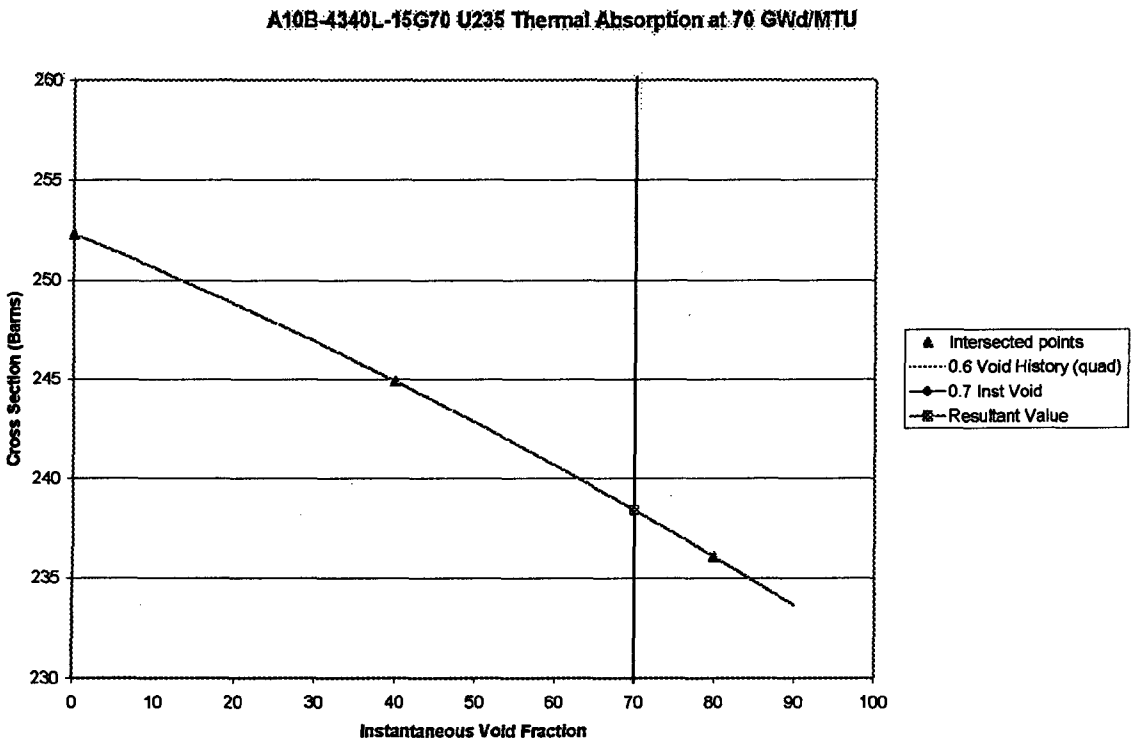

Figure SRXB-A.34-11: Comparison of k-infinity from MICROBURN-B2 Interpolation Process with CASMO-4 Calculations at Intermediate Void Fractions of 0.2, 0.6 and 0.9

[[

]]

Figure SRXB-A.34-12: Comparison of k-infinity from MICROBURN-B2 Interpolation Process with CASMO-4 Calculations at 0.4 Historical Void Fractions and 0.9 Instantaneous Void Fraction

[[

]]

Figure SRXB-A.34-13: Delta k-infinity from MICROBURN-B2 Interpolation Process with CASMO-4 Calculations at 0.4 Historical Void Fraction and 0.9 Instantaneous Void

[[

]]

Figure SRXB-A.34-14: Comparison of Interpolation Process Using Void Fractions of 0.0, 0.4 and 0.9 and Void Fractions of 0.0, 0.45 and 0.9

[[

]]

NRC Request SRXB-A.35

Provide qualitative description of the void data base and the associated correlation. Specifically, describe the uncertainty associated with the data gathering, identifying the uncertainties currently applied to the void fraction correlation and justify its applicability for EPU conditions.

TVA Reply to SRXB-A.35 - Revised

The Zuber-Findlay drift flux model (Reference SRXB-A.35-1) is utilized in the FANP nuclear and safety analysis methods for predicting vapor void fraction in the BWR system. The model has a generalized form that may be applied to two phase flow by defining an appropriate correlation for the void concentration parameter, Co, and the drift flux, Vgj. The model parameters account for the radially non-uniform distribution of velocity and density and the local relative velocity between the phases, respectively. This model has received broad acceptance in the nuclear industry and has been successfully applied to a host of different applications, geometries, and fluid conditions through the application of different parameter correlations (Reference SRXB-A.35-2).

Two different correlations are utilized at FANP to describe the drift flux parameters for the analysis of a BWR core. The correlations and treatment of uncertainties are as follows:

- The nuclear design, frequency domain stability, nuclear AOO transient, and accident analysis methods use the [[ ]] void correlation (Reference SRXB-A.35-3) to predict nuclear parameters. Uncertainties are addressed at the overall methodology and application level rather than individually for the individual correlations of each method. The overall uncertainties are determined statistically by comparing predictions using the methods against measured operating data for the reactors operating throughout the world.

- The thermal-hydraulic design, system AOO transient and accident analysis, and loss of coolant accident (only at specified junctions) methods use the Ohkawa-Lahey void correlation (Reference SRXB-A.35-4). This correlation is not used in the direct computation of nuclear parameters in any of the methods. Uncertainties are addressed at the overall methodology level through the use of conservative assumptions and biases to assure uncertainties are bounded.

The [[ ]] void correlation was developed for application to multi-rod geometries operating at typical BWR operating conditions using multi-rod data and was also validated against simple geometry data available in the public domain. The correlation was defined to be functionally dependent on the mass flux, hydraulic diameter, quality, and fluid properties.

The multi-rod database used in the [[

]]. As a result, the multi-rod database and prediction uncertainties are not available to FANP. However, the correlation has been independently validated by FANP against public domain multi-rod data and proprietary data collected for a prototypical ATRIUM-10 test assembly. Selected results for the ATRIUM-10 test assembly are reported in the public domain in Reference SRXB-A.35-5.

The Ohkawa-Lahey void correlation was developed for application in BWR transient calculations. In particular, the correlation was carefully designed to predict the onset of counter-current flow limit characteristics during the occurrence of a sudden inlet flow blockage. The correlation was defined to be functionally dependent on the mass flux, quality, and fluid properties.

Independent validation of the correlation was performed by FANP at the request of the NRC during the Licensing Topical Report review of the XCOBRA-T code. The NRC staff subsequently reviewed and approved Reference SRXB-A.35-6, which compared the code to a selected test from the FRIGG experiments (Reference SRXB-A.35-7). More recently the correlation has been independently validated by FANP against additional public domain multi-rod data and proprietary data collected for a prototypical ATRIUM-10 test assembly.

The characteristics of the FANP multi-rod void fraction validation database are listed in Table SRXB-A.35-1.

The FRIGG experiments have been included in the validating database because of the broad industry use of these experiments in benchmarking activities, including TRAC, RETRAN, and S-RELAP5. The experiments include a wide range of pressure, subcooling, and quality from which to validate the general applicability of a void correlation. However, the experiments do not contain features found in modern rod bundles such as part length fuel rods and mixing vane grids. The lack of such features makes the data less useful in validating correlations

for modern fuel designs. Also, the reported instrument uncertainty for these tests is provided in Table SRXB-A.35-1 based on mockup testing. However, the total uncertainty of the measurements (including power and flow uncertainties) is larger than the indicated values.

Because of its prototypical geometry, the ATRIUM-10 void data collected at KATHY was useful in validating void correlation performance in modern rod bundles that include part length fuel rods, mixing vane grids, and prototypic axial/radial power distributions. Void measurements were made at one of three different elevations in the bundle for each test point: just before the end of the part length fuel rods, midway between the last two spacers, and just before the last spacer.

As shown in Figure SRXB-A.35-1, the range of conditions for the ATRIUM-10 void data is valid for typical reactor conditions. This figure compares the equilibrium quality at the plane of measurement for the ATRIUM-10 void data with the exit quality of bundles in the EMF-2158 benchmarks and BFN operating at EPU (including MELLLA+) conditions. As seen in the figure, the data at the measurement plane covers nearly the entire range of reactor conditions. However, calculations of the exit quality from the void tests show the overall test conditions actually envelope the reactor conditions. (Note, the ATRIUM-10 data shown in Figure SRXB-A.35-1 is not from the same database as illustrated in Figure SRXB-A.15-1.)

Figures SRXB-A.35-2 and 35-3 provide comparisons of predicted versus measured void fractions for the FANP multi-rod void fraction validation database using the [[ ]] correlation. These figures show the predictions fall within ±0.05 (predicted - measured) error bands with good reliability and with very little bias. Also, there is no observable trend of uncertainty as a function of void fraction.

Figures SRXB-A.35-4 and 35-5 provide comparisons of predicted versus measured void fractions for the FANP multi-rod void fraction validation database using the Ohkawa-Lahey correlation. This same data is presented in a Void/Quality profile in Figures SRXB-A.35-6 and 35-7. In general, the correlation predicts the void data with a scatter of about ±0.05 (predicted - measured), but a bias in the prediction is evident for voids between 0.5 and 0.8. The observed under prediction is consistent with the observations made in Reference SRXB-A.35-6.

In conclusion, validation using the FANP multi-rod void fraction validation database has shown that both drift flux correlations remain valid for modern fuel designs. Furthermore, there is no observable trend of uncertainty as a function of void fraction. This shows there is no increased uncertainty in the prediction of nuclear parameters at EPU (including MELLLA+) conditions within the nuclear methods as a result of changes to the population distribution of the nodal void fractions with respect to pre EPU conditions (See response to SRXB-A.27 for the pre-EPU and EPU void distributions.).

References:

SRXB-A.35-1: N. Zuber and J. A. Findlay, "Average Volumetric Concentration in Two-Phase Flow Systems," J. Heat Transfer, 1965

SRXB-A.35-2: P. Coddington and R. Macian, A Study of the Performance of Void Fraction Correlations Used in the Context of Drift-Flux Two-Phase Flow Models," Nuclear Engineering and Design, 215, 199-216

SRXB-A.35-3: [[

]]

SRXB-A.35-4: K. Ohkawa and R. T. Lahey, Jr., "The Analysis of CCFL Using Drift-Flux Models,"Nuclear Engineering and Design, 61, 1980

SRXB-A.35-5: S. Misu et al., "The Comprehensive Methodology for Challenging BWR Fuel Assembly and Core Design used at FANP," proceedings on CD-ROM, PHYSOR 2002, Seoul, Korea, October 7-10, 2002

SRXB-A.35-6: XN-NF-84-105(P)(A) Volume 1 Supplement 4, "XCOBRA-T: A Computer Code For BWR Transient Thermal-Hydraulic Core Analysis, Void Fraction Model Comparison to Experimental Data," Advanced Nuclear Fuels Corporation, June 1988

SRXB-A.35-7: O. Nylund et al., "Hydrodynamic and Heat Transfer Measurements on a Full-Scale Simulated 36-Rod Marviken Fuel Element with Non-Uniform Radial Heat Flux Distribution," FRIGG-3, R 494/RL-1154, November 1969

SRXB-A.35-8: J. Skaug et al., "FT-36b, Results of Void Measurements," FRIGG-PM-15, May 1968

SRXB-A.35-9: O. Nylund et al., "Hydrodynamic and Heat Transfer Measurements on a Full-Scale Simulated 36-Rod Marviken Fuel Element with Eniform Heat Flux Distribution," FRIGG-2, R 447/RTL-1007, May 1968

SRXB-A.35-10: AIC-1308656-1, "Initial Void Measurements at the Karlstein Thermal Hydraulic Test Loop," FANP, April 2003

Table 35-1: FANP Multi-Rod Void Fraction Validation Database

	FRIGG-2 (Reference SRXB-A.35-9)	FRIGG-3 (Reference SRXB-A.35-7 and -8)	ATRIUM-10-KATHY (Reference SRXB-A.35-10)
Axial Power Shape	uniform	uniform	[[ ]]
Radial Power Peaking	uniform	mild peaking	[[ ]]
Bundle Design	circular array with 36 rods + central thimble	circular array with 36 rods + central thimble	prototypical ATRIUM-10 CHF bundle
Pressure (psi)	725	725, 1000, and 1260	[[ ]]
Inlet Subcooling (^{0}F)	4.3 to 40.3	4.1 to 54.7	[[ ]]
Mass Flow Rate (lbm/s) *(calculated from mass flux assuming ATRIUM-10 inlet flow area)*	14.3 to 31.0	10.1 to 42.5	[[ ]]
Equilibrium Quality at Measurement Plane (fraction)	-0.036 to 0.203	-0.058 to 0.330	[[ ]]
Max Void at Measurement Plane (fraction)	0.828	0.848	[[ ]]
Reported Instrument Uncertainty (fraction)	0.025	0.016	[[ ]]
Number of Data	27 tests, 174 points	39 tests, 157 points	[[ ]]

Figure SRXB-A.35-1: Comparison of the Measured Local Quality for ATRIUM-10 Void Data and Exit Quality for Typical Reactor Conditions

[[

]]

Figure SRXB-A.35-2: Validation of [[ ]] using FRIGG-2 and FRIGG-3 Void Data

[[

]]

Figure SRXB-A.35-3: Validation of [[ ]] using ATRIUM-10 Void Data

[[

]]

Figure SRXB-A.35-4: Validation of Ohkawa-Lahey using FRIGG-2 and FRIGG-3 Void Data

[[

]]

Figure SRXB-A.35-5: Validation of Ohkawa-Lahey using ATRIUM-10 Void Data

[[

]]

Figure SRXB-A.35-6: Validation of Ohkawa-Lahey using FRIGG3 Void Data at 50 bar

[[

]]

Figure SRXB-A.35-7: Validation of Ohkawa-Lahey using ATRIUM-10 Void Data at 69 bar

[[

]]